# Morphology and Topochemical Reactions of Novel Vanadium Oxide Nanotubes

**F. Krumeich,[†] H.-J. Muhr,[†] M. Niederberger,[†] F. Bieri,[†] B. Schnyder,[‡] and R. Nesper*,[†]**

*Contribution from the Laboratory of Inorganic Chemistry, Swiss Federal Institute of Technology (ETH), Universitätstrasse 6, CH-8092 Zürich, Switzerland, and Electrochemistry Section, Paul Scherrer Institute, CH-5232 Villigen PSI, Switzerland*

*Received April 5, 1999*

**Abstract:** Vanadium oxide nanotubes were obtained as the main product in a sol−gel reaction followed by hydrothermal treatment from vanadium(V) alkoxide precursors and primary amines ($C_nH_{2n+1}NH_2$ with $4 \leq n \leq 22$) or $\alpha,\omega$-diamines ($H_2N[CH_2]_nNH_2$ with $14 \leq n \leq 20$). The structure of the nanotubes has been characterized by transmission electron microscopy, X-ray powder diffraction, X-ray photoelectron spectroscopy, and magnetic measurements. The tubes are up to 15 $\mu$m long and have outer diameters ranging from 15 to 150 nm and inner diameters from 5 to 50 nm. The tube walls consist of 2−30 crystalline vanadium oxide layers with amine or diamine molecules intercalated in between. The distance between the layers (1.7−3.8 nm) is proportional to the length of the alkylamine, which acts as a structure-directing template. The structure within the layers has a square metric with $a \approx 0.61$ nm. Cross-sectional TEM images demonstrate the predominance of serpentine-like scrolls rather than of concentric tubes. The intercalated templates can be easily substituted, e.g. by diamines, while the tubular morphology is preserved. This points to a highly flexible structure.

## Introduction

For many years, vanadium oxides and derived compounds have attracted special attention because of their outstanding structural flexibility combined with chemical and physical properties which are of interest for, e.g., catalytic and electrochemical applications. While vanadium oxide phases with mixed valency ($VO_x$ with $2.0 < x < 2.5$), containing $V^{5+}$ as well as $V^{4+}$ cations, crystallize in three-dimensional network structures, $V_2O_5$ can be regarded as a layered structure in which $VO_5$ square pyramids are connected by sharing corners and edges and thereby form the layers.[1] The interactions between these layers are rather weak, as indicated by the exceptionally long V−O distance of 0.279 nm.[2] This structural particularity permits the synthesis of phases $M_xV_2O_5$ with various metal cations embedded between the layers without a far-reaching restructuring.[3] Furthermore, the intercalation of tetramethylammonium cations, leading to a similar structure, can be achieved by hydrothermal synthesis.[4] Meanwhile, a lot of new complex vanadium oxides have been prepared by this "chimie douce" method, which, although well-established for the syntheses of, e.g., zeolites and mesoporous alumosilicates,[5] represents a rather new approach in this system.

In many of these hydrothermally synthesized vanadium oxides, which contain different metal or organic cations, $VO_4$ tetrahedra appear together with the typical $VO_5$ square pyramides.[6] This fact as well as the presence of various amounts of $V^{4+}$ besides $V^{5+}$ contributes to the multitude of imaginable or already obtained structures. In the course of the hydrothermal synthesis, the reaction path is very sensitive to the actually applied experimental conditions, e.g., temperature, pH, and duration of the hydrothermal treatment. It is of special practical importance that the reaction can be controlled by the selection of suitable organic molecules which act as templates, directing the formation of a structure toward a desired target arrangement. Such a ligand-assisted templating approach was used for the preparation of mesoporous transition metal oxides such as Nb-TMS1[7] and Ta-TMS1.[8] In these compounds, the amine surfactants are covalently bound via their headgroups to discrete inorganic precursor units (metal alkoxides).

Recently, we obtained a novel tube-shaped vanadium oxide with mixed valency on a similar route by intercalation of primary alkylamines.[9] There are only a few examples of solids crystallizing with such a tubular morphology. Long known prototypes are silicate minerals such as serpentine.[10] Nanoparticles of various layered compounds which crystallize in fullerene-like hollow-cage structures also form nanotubes under certain experimental conditions. Dichalcogenides (i.e., $MoS_2$, $WS_2$,[11] and $NiCl_2$[12]) are examples for this growth behavior.[13] The carbon

* To whom correspondence should be addressed. E-mail: nesper@inorg.chem.ethz.ch.

† ETH Zürich.

‡ Paul Scherrer Institute.

(1) Bachmann, H. G.; Ahmed, F. R.; Barnes, W. H. *Z. Kristallogr.* **1961**, *115*, 110.

(2) Enjalbert, R.; Galy, J. *Acta Crystallogr. C* **1986**, *42*, 1467.

(3) Galy, J. *J. Solid State Chem.* **1992**, *100*, 229.

(4) Wittingham, M. S.; Guo, J.; Chen, R.; Chirayil, T.; Janauer, G.; Zavalij, P. *Solid State Ionics* **1995**, *75*, 257.

(5) Beck, J. S.; Vartuli, J. C.; Roth, W. J.; Leonowicz, M. E.; Kresge, C. T.; Schmitt, K. D.; Chu, C. T.-W.; Olson, D. H.; Sheppard, E. W.; McCullen, S. B.; Higgins, J. B.; Schlenker, J. C. *J. Am. Chem. Soc.* **1992**, *114*, 10834.

(6) Chirayil, T.; Zavalij, P. Y.; Wittingham, M. S. *Chem. Mater.* **1998**, *10*, 2629.

(7) Antonelli, D. M.; Nakahira, A.; Ying, J. Y. *Inorg. Chem.* **1996**, *35*, 3126.

(8) Antonelli, D. M.; Ying, J. Y. *Chem. Mater.* **1996**, *8*, 874.

(9) (a) Nesper, R.; Spahr, M. E.; Niederberger, M.; Bitterli, P. Int. Patent Appl. PCT/CH97/00470, Bundesamt für Geistiges Eigentum, Bern, 1997. (b) Spahr, M. E.; Bitterli, P.; Nesper, R.; Müller, M.; Krumeich, F.; Nissen, H.-U. *Angew. Chem., Int. Ed. Engl.* **1998**, *37*, 1263. (c) Nesper, R.; Muhr, H.-J. *Chimia* **1998**, *52*, 571.

(10) Liebau, F. *Structural Chemistry of Silicates*; Springer-Verlag, Berlin, 1985.

(11) Tenne, R.; Homyonfer, M.; Feldman, Y. *Chem. Mater.* **1998**, *10*, 3225.

(12) Rosenfeld Hacohen, Y.; Grunbaum, E.; Tenne, R.; Sloan, J.; Hutchison, J. L. *Nature* **1998**, *395*, 336.

nanotubes, discovered by Iijima in 1991,[14] are at present in the focus of worldwide investigations because of their unique structural and physical properties[15] which render applications as multifunctional nanodevices possible.[16] The discovery of a further example for this particular morphology in the form of modified vanadium oxides represents a major step forward because these materials are easily accessible in gram quantities as the main reaction product under soft chemical conditions. Here, we focus on the morphology and topochemical reactions of as-synthesised and diamine-exchanged VO$_x$−NTs,[17] which we termed ETH1 according to the usual practice of denotation for mesoporous materials.[9b]

## Experimental Section

**Preparation.** A solution of vanadium(V) triisopropoxide and a primary amine (C$_n$H$_{2n+1}$NH$_2$ with $4 \leq n \leq 22$) or a α,ω-diamine (H$_2$N-[CH$_2$]$_n$NH$_2$ with $14 \leq n \leq 20$) in a molar ratio of 2:1 in absolute ethanol (3 mL/g of vanadium precursor) was stirred under inert atmosphere for 1 h. The resulting yellow solution of the alkoxide−amine adduct was hydrolyzed with water (5 mL/g of vanadium precursor) under vigorous stirring. After aging (12−96 h), an orange composite of surfactant and hydrolyzed vanadium oxide component was obtained. The hydrothermal reaction of this composite in an autoclave at 180 °C (2−7 d) resulted in a black product. It was finally washed with ethanol and hexane to remove residues of unreacted amine or decomposition products and then dried at 80 °C (1 d) under vacuum. TEM and X-ray powder diffraction investigations reveal that, after this purification, the product is phase-pure, consisting of tubes only. These samples were used as well for quantitative chemical analyses on vanadium, carbon, hydrogen, and nitrogen (Table 1).

The exchange reactions were performed by stirring a suspension of the tubes (about 100 mg) in 25 mL of ethanol with an excess of the exchanging diamine H$_2$N[CH$_2$]$_n$NH$_2$ with $2 \leq n \leq 20$ (about 1 mole equiv with respect to the amount of monoamine in the tubes, i.e., two monoamine molecules are exchanged against one diamine molecule) for 12 h at room temperature (Table 3).

Most chemicals were purchased from Fluka (vanadium(V) triiospropoxide from ABCR) and used without further purification. Amines with $n = 20$, 22 and all diamines have been prepared applying different standard synthesis procedures.

**X-ray Powder Diffraction.** The X-ray powder diffraction (XRD) diagrams of all samples were measured in the transmission mode (0.3 mm glass capillaries, CuKα$_1$ radiation) on a STOE STADI−P2 diffractometer equipped with a position-sensitive detector with a resolution of about 0.01° in 2Θ.

**X-ray Photoelectron Spectroscopy.** The nanotubes were further characterized by X-ray photoelectron spectroscopy (XPS) on a ES-CALAB 220i XL (VG Scientific). To have a better energy resolution, a monochromatized X-ray source was used (Al Kα$_1$ radiation, 200 W (10 kV, 20 mA)).

(13) It should be noted that fullerene-like structures were found in VS$_2$ nanoparticles obtained by sulfidization of V$_2$O$_5$ (Homyonfer, M.; Alperson, B.; Rosenberg, Y.; Sapir, L.; Cohen, S. R.; Hodes, G.; Tenne, R. *J. Am. Chem. Soc.* **1997**, *119*, 2693).

(14) Iijima, S. *Nature* **1991**, *354*, 56.

(15) (a) Wildöer, J. W.; Venema, L. C.; Rinzler, A. G.; Smalley, R. E.; Dekker: C. *Nature* **1998**, *391*, 59. (b) Odom, T. W.; Huang, J. L.; Kim, P.; Lieber, C. M. *Nature* **1998**, *391*, 62. (c) Falvo, M. R.; Clary, G. J.; Taylor, R. M., II; Chi, V.; Brooks, F. P., Jr.; Washburn, S.; Superfine, R. *Nature* **1997**, *389*, 582.

(16) (a) Dillon, A. C.; Jones, K. M.; Bekkedahl, T. A.; Kiang, C. H.; Bethune, D. S.; Heben, M. J. *Nature* **1997**, *386*, 377. (b) Che, G.; Lakshmi, B. B.; Fisher, E. R.; Martin, C. R. *Nature* **1998**, *393*, 346. (c) Wong, E. W.; Sheehan, P. E.; Lieber, C. M. *Science* **1997**, *277*, 1971. (d) Wong, S. S.; Joselevich, E.; Woolley, A. T.; Cheung, C. L.; Lieber, C. M. *Nature* **1998**, *394*, 52. (e) Tans, S. J.; Verschueren, A. R. M.; Dekker, C. *Nature* **1998**, *393*, 49. (f) Ugarte, D.; Châtelain, A.; de Heer, W. A. *Science* **1996**, *274*, 1897.

(17) In the following, vanadium oxide nanotubes are designated as C$_n$−VO$_x$−NTs with alkylmonoamine templates ($n$ = number of CH$_2$ groups) or as C$_n$−DA−VO$_x$−NTs with α,ω-alkyldiamine templates ($n$ = number of CH$_2$ groups).

**Magnetic Measurements.** Magnetic susceptibilities were measured on a squid magnetometer (MPMS 5S, Quantum Design) at a field of 1 T at room temperature. To avoid texture effects due to the large anisotropy of the material, the quartz sample holder was rotated by 360° during the measurements. The samples were fitted in the holder as pellets of 6 mm diameter. Selective temperature-dependent measurements showed that there is no Curie−Weiss behavior. Thus, only effective magnetic moments have been calculated. The magnetism has to be traced back to V$^{4+}$ centers, which compared to pure vanadium-(IV) compounds are assumed to be fairly separated, i.e., even less than in the latter, coupling between the centers is expected. The measured effective moment of selected vanadium(IV) compounds, e.g., VCl$_4$ and VOSO$_4$·3H$_2$O of about 1.6 $\mu_B$ shows that there is a spin−orbit coupling, which reduces the theoretical value of 1.73 $\mu_B$. Therefore, the experimental value of 1.6 $\mu_B$ was used as reference for the calculation of the vanadium(IV) contents.

**Transmission Electron Microscopy.** Transmission electron microscopy (TEM) investigations were performed on a CM30ST microscope (Philips; LaB$_6$ cathode, operated at 300 kV). For the investigation of the longitudinal shape and structure, the nanotube material was deposited onto a perforated carbon foil supported on a copper grid. To observe the structure perpendicular to the tube axis, a cross-sectional preparation technique was applied. The VO$_x$−NTs were deposited on a Si wafer coated with an epoxy resin and then covered with a second Si wafer. Most of the tubes were now oriented flat between the wafers. This "sandwich" was put into a copper tube (outer diameter 3 mm), which was then filled with epoxy. After the resin was hardened, the resulting cylinder was cut into slices (thickness ≈300 $\mu$m) which were then mechanically abraded on both sides to a thickness between 100 and 150 $\mu$m. Subsequently, dimples (depth ≈ 40−60 $\mu$m) were ground into both sides of the slice (Dimple Grinder, Gatan). In the final preparation step, the specimen was etched on both sides with ion beams (PIMS, Gatan, argon ions, 4 keV) until a hole was created in the central area containing the tubes. At the thin specimen edge close to the hole, the tubes can be observed by TEM, and their orientation quite often allows an investigation along the tube axis. The element-specific images were obtained by means of the electron spectroscopic imaging technique with an energy filter (Gatan imaging filter) installed at a CM200ST FEG microscope (Philips; field emission gun, operated at 200 kV).

## Results and Discussion

Aliphatic primary amines with alkyl chain lengths within a large size range (between 4 and 22 CH$_2$ groups) can be used as templates for the preparation of VO$_x$−NTs. The variety of chain lengths in the case of aliphatic α,ω-diamine templates (H$_2$N-(CH$_2$)$_n$NH$_2$) is more limited and extends only from $n = 14$ to 20. Further decrease of the chain length predominantly leads to vanadium oxide fibers ($n = 12$) or to lamellar structured composites with irregular shape ($n = 4$).

The initial molar vanadium-to-monoamine ratio (V/template ratio) was varied from 4 to 1 while the amounts of water for hydrolysis and ethanol for dissolution of the vanadium alkoxide−monoamine complex were kept constant. VO$_x$−NTs were obtained at V/template ratios ranging from 3 to 2, whereas a further decrease of the template content (ratio = 4) led to the formation of lamellar structured products. Well-developed VO$_x$−NTs with α,ω-diamines as structure-directing agents were obtained at a V/template ratio of 2. A lower template content (ratio = 3) increased the amount of amorphous byproducts, and at a ratio of 4 only lamellar structured, ribbonlike composites were observed.

Several experiments were performed to investigate the effect of temperature and duration variations on the morphology of the final product. In both cases, i.e., with monoamine or diamine templates, VO$_x$−NTs are only obtained at a temperature of 180 °C within 2 to 7 days. Extended periods of aging at room temperature (e.g., 4 d) shorten the reaction time at 180 °C

**Table 1.** Elemental Compositions, Magnetic Moments, and Layer Distances of As-Synthesized $VO_x$−NTs Obtained with Alkylmonoamine Templates of Different Chain Lengths and an Initial Molar Vanadium(V) Alkoxide/Template Ratio of 2[a]

| | template | $\mu_{eff}$(RT) [$\mu$B] | % $V^{4+}$ | composition | dev $Z$ [g/mol] | layer distance (nm) XRD | ED |
|---|---|---|---|---|---|---|---|
| I | butylamine | 1.16 | 45 | $VO_{2.40}[C_4H_{12}N]_{0.26}$ | 5.6 | 1.66 | 1.58 |
| | hexylamine | 1.41 | 66 | $VO_{2.30}[C_6H_{16}N]_{0.27}$ | 6.4 | 1.96 | 1.62 |
| | decylamine | 0.99 | 33 | $VO_{2.47}[C_{10}H_{24}N]_{0.27}$ | 1.6 | 2.50 | 2.17 |
| | undecylamine | 1.20 | 48 | $VO_{2.40}[C_{11}H_{26}N]_{0.27}$ | 4.8 | 2.59 | 2.16 |
| II | dodecylamine | 1.17 | 45 | $VO_{2.40}[C_{12}H_{28}N]_{0.26}$ | 0.00 | 2.77 | 2.21 |
| | tetradecylamine | 1.13 | 42 | $VO_{2.42}[C_{14}H_{32}N]_{0.27}$ | −0.32 | 3.02 | 2.43 |
| | hexadecylamine | 1.03 | 35 | $VO_{2.45}[C_{16}H_{36}N]_{0.26}$ | 0.00 | 3.20 | 2.63 |
| | octadecylamine | 1.25 | 52 | $VO_{2.37}[C_{18}H_{40}N]_{0.26}$ | 0.48 | 3.48 | 2.86 |
| | eiscosylamine | b | b | $VO_{2.53}[C_{20}H_{43}N]_{0.28}$[c] | | 3.67 | 2.97 |
| | docosylamine | 1.18 | 46 | $VO_{2.42}[C_{22}H_{47}N]_{0.30}$ | −1.12 | 3.80 | 3.15 |

[a] Each effective magnetic moment $\mu_{eff}$ at room temperature (RT) was calculated on the basis of the molecular weight of the sample determined by elemental analysis. The amount of oxygen ($x$) in the elemental composition was determined by the V(IV)/V(V) ratio; the positive charge of the template molecule was counterbalanced by an additional, appropriate amount of doubly charged oxygen anions ($y/2$), thus leading to the general formula $VO_xO_{y/2}[C_nH_{2n+4}N]_y$. The deviation $Z$ means the difference in molecular weight of the elemental compositions with different oxygen amounts either determined by the vanadium(IV) content or calculated from elemental analysis with respect to 100%. The layer distances are determined from the $d$ values of the 00$l$ reflections in X-ray (XRD) and electron diffraction (ED) patterns. Both values are given for comparison  [b] Not measured. [c] Composition from elemental analysis with a calculated amount of oxygen.
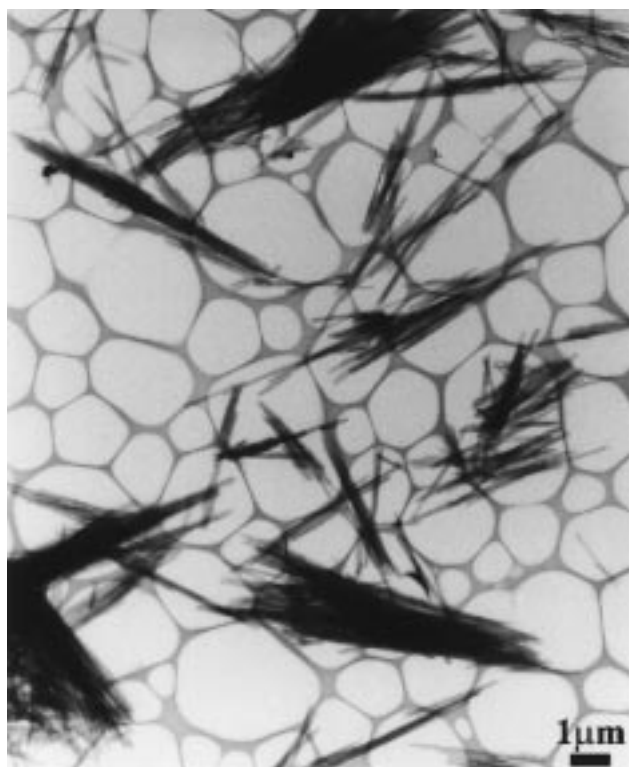


**Figure 1.** Representative TEM image of eicosylamine vanadium oxide nanotubes ($C_{20}$−$VO_x$−NT) with lengths ranging from 3 to 10 $\mu$m. Besides isolated tubes, there are bundles of tubes which are grown together.

(2 d). Remarkably, lower synthesis temperatures ($T = 140$−160 °C) as well as shorter periods of aging at room temperature or of hydrothermal treatment at 180 °C resulted only in lamellar structured composites, whereas heating at higher temperatures ($T > 200$ °C) led, according to X-ray powder diffraction, to the formation of a dense form of vanadium oxide, which has not been further investigated yet.

The reaction products consist almost exclusively of vanadium oxide nanotubes (Figure 1). $VO_x$−NTs are frequently grown together in the form of bundles. Lengths and diameters of the tubes depend on the conditions selected for the preparation, e.g., concentration and type of template, although a large variation has been observed in all experiments (cf. Figure 1). The maximum tube length that has been found up to now is 15 $\mu$m.

On the basis of the effective magnetic moments (cf. Table 1), the relative V(IV) contents were calculated. They show a certain spread around the mean value of 46%. The values of most samples are quite close to the average. It is not yet clear whether the extreme variations for $C_6$−$VO_x$−NTs and $C_{10}$−$VO_x$−NTs, respectively, are due to materials properties or to experimental errors. Based on the mixed valencies, oxygen contents have been calculated. In addition, a surplus has to be added, which compensates for the positive charge of the template molecules. The protonation of the amine has been proved by XPS investigations of $C_{16}$−$VO_x$−NTs and $C_{20}$−$VO_x$−NTs: the N(1s) core level energy (401.5 and 401.6 eV) of the cation is higher than that of unprotonated alkylamine (399.6 and 399.3 eV) and corresponds to a positively charged nitrogen.[18] Independently, cation exchange reactions on $C_{12}$−$VO_x$−NTs and $C_{16}$−$VO_x$−NTs show that between 70 and 90% of the template can be exchanged by different cations (see below and ref 23). At least this amount of the template is expected to be protonated.

According to elemental analysis (Table 1) and geometrical considerations, the $VO_x$−NTs with monoamines in the whole size range $4 \leq n \leq 22$ can be divided into two sections. We assume that the cationic part of the ammonium templates is directed toward the vanadium oxide layers. For section I ($4 \leq n \leq 11$), the observed layer distances (XRD, cf. Table 1 and inset in Figure 5) are larger than twice the calculated maximum lengths of the alkylammonium templates. This indicates that the ends of the aliphatic chains only touch or slightly overlap. At the same time, there are some weight differences with respect to 100% ($Z$, Table 1), which may be attributed to additional incorporated species. However, this effect needs further investigation. For section II ($12 \leq n \leq 22$), the observed layer distances, which are smaller than the calculated length of the amines (inset in Figure 5), imply that a considerable overlap of

(18) The N(1s) core level energy at 402.0 eV of the positively charged nitrogen in trimethylhexadecylammoniumbromid (Zhao, W. W.; Boerio, F. J. *Surf. Interface Anal.* **1998**, *26*, 316) is similar to that of the $VO_x$−NTs. This agreement clearly reveals the protonation of the amine template.

(19) Reimer, L. *Energy-Filtering Transmission Electron Microscopy*; Springer-Verlag: Berlin 1995; pp 347−400.

(20) Lagaly, G. *Solid State Ionics* **1986**, *22*, 43.

(21) Wörle, M.; Krumeich, F.; Brändle, M.; Muhr, H.-J.; Nesper R. To be submitted for publication.

(22) We index the XRD pattern on the basis of a lattice with $a = b = 0.611$ nm, $c = 2.74$ nm. The angle between the $a$−$b$ plane and the $c$ axis differs from 90° and is variable due to different curvatures of the layers (see text).

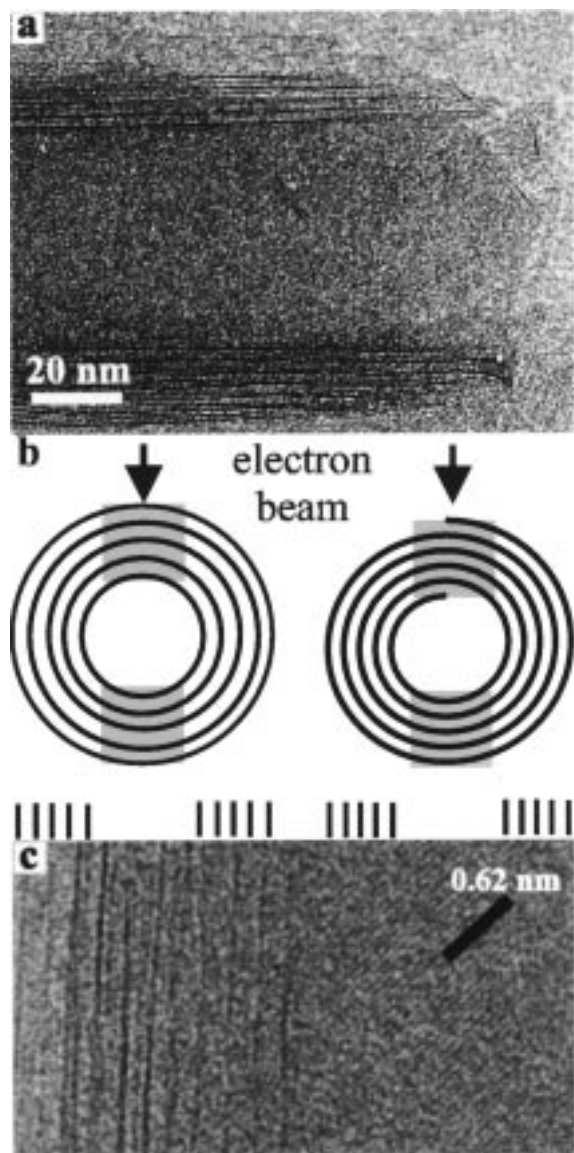(23) Reinoso, M. Diploma Thesis, ETH Zurich, 1999.

**Figure 2.** (a) TEM image of a typical nanotube (C$_{12}$−VO$_x$−NT), showing the multilayered wall structure with a distance of ∼2.3 nm between the layers. The inner diameter is ∼45 nm, the outer one ∼80 nm. (b) Schematic cross-sectional representations of a concentric shell tube (left) and a scroll-tube (right) and of their interaction with the electron beam (see text). (c) HRTEM image of a part of a VO$_x$−NT nanotube. Dark fringes at the left side are caused by the VO$_x$ layers inside the tube walls. At the right side a region corresponding to those in gray in panel b is shown. The structure within the layers gives rise to a pattern of parallel lines with a distance of 0.62 nm at an angle of 45° with respect to the tube walls.

the aliphatic tails and/or large tilt angles (up to 50°) must be present. A tilt angle of 0° corresponds to an orientation of the template molecules perpendicular to the oxidic layers.

The elemental compositions, i.e., the vanadium, oxygen, and template contents, are found to be within a fairly small range with the general formula VO$_{2.39\pm0.09}$(C$_n$H$_{2n+4}$N)$_{0.27\pm0.01}$ for range I and VO$_{2.45\pm0.08}$(C$_n$H$_{2n+4}$N)$_{0.27\pm0.01}$ for range II. This is rather striking if one considers that the precursor material contains exclusively V(V) centers which for all templates are partially reduced to the same narrow range of mixed valency. It is thus quite likely that a specific average oxidation state of vanadium is essential for the tube formation.

The tubular structure is evident from TEM images. The tube shown in Figure 2a has an open end and an outer diameter of approximately 80 nm. The walls appear as alternating fringes of dark and bright contrast. The dark contrast of the narrow fringes indicates that atoms with high scattering potential are concentrated there. Therefore, these layers contain the vanadium atoms, which are by far the strongest scatterers in this compound. Between these vanadium oxide layers, the amine molecules are embedded. This structural model is confirmed by the results of electron spectroscopic imaging[19] of cross-sections (Figure 3). The bright contrast in the vanadium map (Figure 3b), which indicates the presence of V, appears exactly at the same sites as the dark contrast in the TEM image (Figure 3a). Furthermore, the carbon map (Figure 3c) shows that C (bright) is present between these VO$_x$ layers (dark) and, thus, that the template molecules are located there. The surroundings of the tubes also appear bright owing to the organic embedding material (cf. Experimental Section).

The average distance between the VO$_x$ layers in the tube walls gives rise to corresponding reflections in the diffraction patterns (Figures 4 and 5). In electron diffraction patterns (Figure 4), rows of sharp reflections with narrow distances are present close to the direct beam. This observation indicates that the layers inside the walls are indeed well-ordered and equidistantly arranged with respect to each other. In projection along the incident electron beam, the VO$_x$ layers can be regarded as oriented almost parallel to the beam in a certain area (Figure 2b). On one hand, this leads to TEM micrographs with the structure inside tube walls imaged as alternating lines of dark and bright contrasts; on the other hand, this pattern of parallel lines generates a row of spots in reciprocal space, corresponding to the distance between the lines.

The interlayer distances at various alkyl chain lengths of the template determined by powder diffraction can be explained by a monolayer of template molecules in a paraffin-like arrangement between the layers. Such a structure is frequently observed in alkylamine-intercalated layer structures of a large variety of substances.[20] This arrangement of template molecules is flexible and permits numerous exchange reactions without destructing the tubular structure (cf. below).

In addition, further Bragg reflections are present in the electron diffraction patterns, which are arranged on a square lattice with an edge length corresponding to approximately 0.62 nm in real space. These reflections provide information about the structure within the layers. They arise from the gray region in the schematic representation (Figure 2b) where the layers are almost perpendicular to the incident electron beam. Remarkably, this square lattice of reflections appears on the same sites for all C$_n$−VO$_x$ nanotube samples while the distance between the reflections in the central row significantly shifts with the interlayer distance (Table 1). This fact clearly proves that the structure of the VO$_x$ layers is the same in all tubes independent of the template molecule. (This is strong support for the assumption that the oxidation state of vanadium does not change significantly between different samples and that the extreme values of the magnetic measurements may be due to experimental errors). Owing to the bending of the layers as well as to defects inside the nanotube walls, these reflections are always blurred to some extent.

The structure of the tubes in conjunction with their large diameter causes unique electron diffraction patterns that contain three-dimensional structural information despite being only two-dimensional sections of reciprocal space. The central row of spots is rotated by 45° with respect to the square of reflections, indicating a well-defined orientation relationship between layer structure and the walls. A TEM image obtained at higher
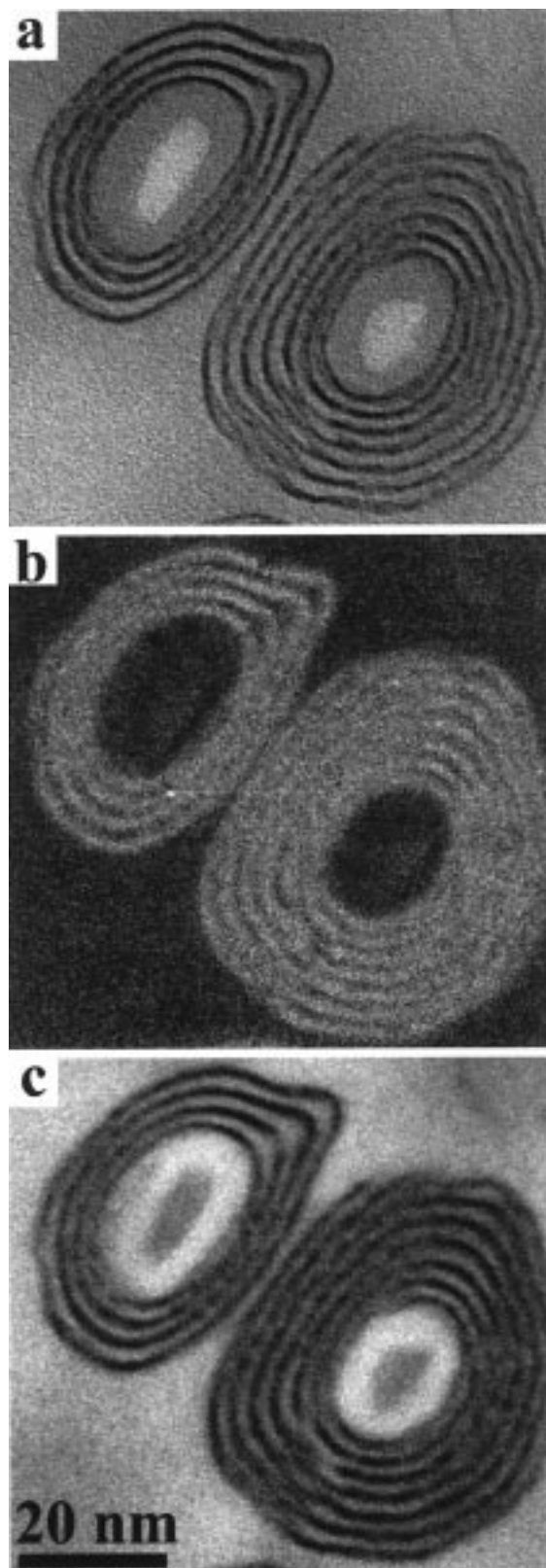
**Figure 3.** (a) Cross-sectional TEM image of $C_{16}-VO_x-NTs$. Elemental distribution images of vanadium (b), using the V_L edge, and of carbon (c), using the C_K edge.
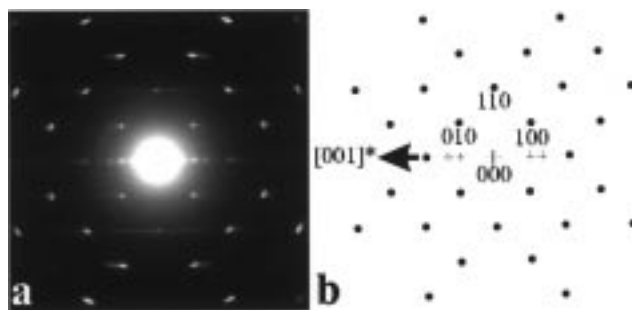


**Figure 4.** (a) Typical selected area electron diffraction pattern of a nanotube. (b) Schematic representation. The reflections $00l$ (symbolized by +) are caused by the regular interlayer distance while the square arrangement of spots $hk0$ (symbolized by ●) corresponds to a square lattice ($a \approx 0.62$ nm) within the layers.
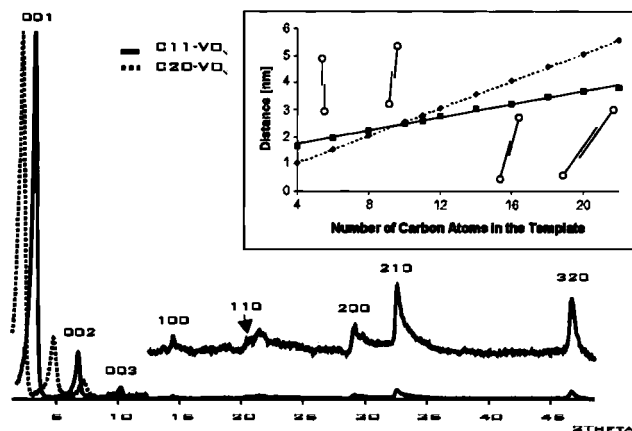


**Figure 5.** X-ray powder diffraction pattern of $VO_x-NTs$ with different interlayer distances. The enlarged section shows the characteristic reflections $hk0$ generated by the structure within the layers, indexed on the basis of a two-dimensional square lattice with $a = 0.61$ nm. These reflections appear at the same sites in all samples independent of the template used. On the other hand, the distance between the layers, generating the reflections $00l$, increases proportional to the length of the carbon chain (solid line in the inset, cf. Table 1). The dotted line represents twice the maximum chain lengths of the alkylammonium templates calculated from increments for the $CH_2$ group. The different inclinations of the solid and the dotted line are discussed in the text.

magnification (Figure 2c) confirms this interpretation: lattice fringes with a distance of about 0.62 nm appear and are indeed rotated by about 45° with respect to the $VO_x$ layers. It should be noted that in the present study electron diffraction normally reveals more structural information about the tube structure than HRTEM images (Figure 2c): while the square structure inside the layers gives rise to corresponding reflections, it is mostly not recognizable in HRTEM images since this part of the structure is modified or even destroyed by the intense electron beam that is necessary to record these images. Only the layer structure of the walls partly withstands this treatment. In the course of the HRTEM investigation, the row of reflections disappeared often or became blurred, indicating an increased disorder. As a matter of fact, Figure 2c represents one of the few images we have obtained up to now where focusing and recording was possible before the structural contrast inside the layers completely disappeared.

The interpretation of the electron diffraction results is confirmed by the evaluation of the X-ray powder patterns (Figure 5): the peak with highest intensity is located at $d$ values between 1.7 and 3.8 nm, and it corresponds to the distance between the $VO_x$ layers. Moreover, a set of less intense peaks appears at smaller $d$ values (cf. Table 2). These reflections are caused by the structure within the layers as revealed by electron diffraction and, thus, can be indexed on the basis of a two-dimensional square lattice with $a \approx 0.61$ nm (Table 2). The absence of reflections of the type $hkl$ with $l \neq 0$ is noteworthy. As the reflections of type $hk0$ as well as of type $00l$ are relatively sharp peaks, it is possible to define an approximate three-
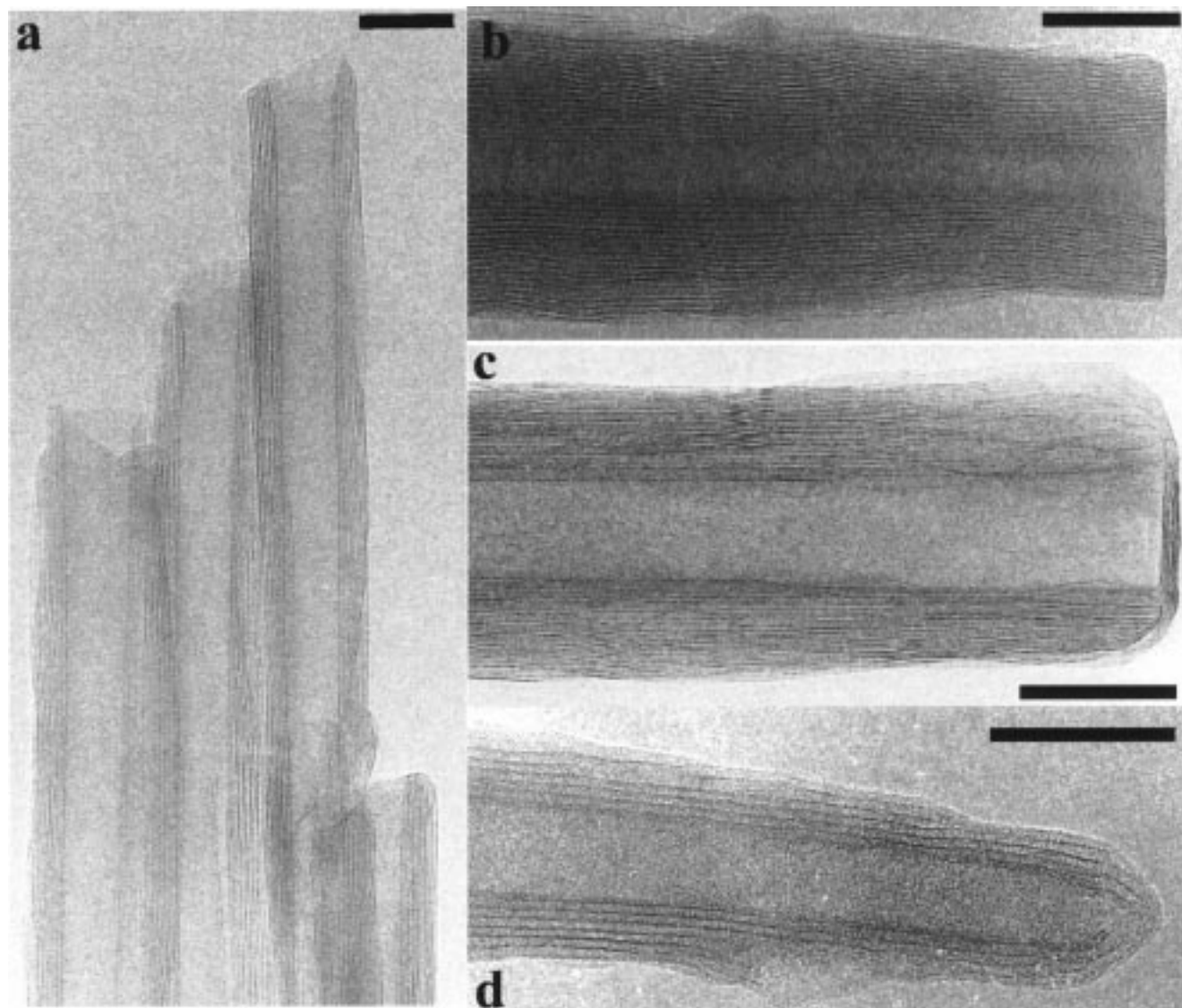
**Figure 6.** TEM images of various nanotubes. (a) C$_{16}$−VO$_x$−NTs and (b) a C$_{20}$−DA−VO$_x$−NT with open ends. (c) C$_4$−VO$_x$−NT and (d) C$_{16}$−VO$_x$−NT with closed ends. In all images, the length of the bar is 50 nm.

**Table 2.** X-ray Powder Diffraction Data of C$_{12}$−VO$_x$−NTs[22]

| diff angle 2Θ [deg] | d value [nm] | [hkl] | diff angle 2Θ [deg] | d value [nm] | [hkl] |
|---|---|---|---|---|---|
| 6.43 | 1.373 | 002[a] | 36.27 | 0.247 | c |
| 9.68 | 0.912 | 003[a] | 39.81 | 0.226 | c |
| 12.95 | 0.683 | 004[a] | 43.35 | 0.209 | 220[b] |
| 14.49 | 0.611 | 100$^2$ | 44.75 | 0.203 | 300[b] |
| 16.15 | 0.548 | 005[a] | 46.76 | 0.194 | 310[b] |
| 19.56 | 0.454 | 006[a] | 53.78 | 0.170 | 320[b] |
| 20.46 | 0.433 | 110 | 60.23 | 0.154 | 400[b] |
| 26.20 | 0.340 | 3 | 62.30 | 0.149 | 330[b] |
| 29.11 | 0.306 | 200[b] | 68.26 | 0.137 | 420[b] |
| 32.61 | 0.274 | 210[b] | | | |

[a] Reflections 00*l* of the layer structure with a calculated distance of 2.74 nm. The reflection 001 was not recorded in this high-resolution measurement. [b] Reflections *hk*0 of the square metric of the structure within the layers with a lattice constant *a* = 0.611 nm. [c] Broad reflections of low intensity which cannot be indexed.

dimensional unit cell despite the bending of the layers. Further structural information derived from the X-ray powder patterns will be given in a subsequent publication.[21]

While the data obtained from the two diffraction methods coincide regarding the characteristic *hk*0 reflections caused by the structure within the layers, there is a certain discrepancy between the *d* values of the 00*l* reflections corresponding to the layer distance. The *d* values of the 001 peaks (1.7−3.8 nm) in the X-ray powder patterns of different samples (Table 1) are always larger than those determined by electron diffraction or derived from longitudinal TEM images. This deviation (0.05−0.65 nm) increases with the length of the templates alkyl chain. Remarkably, this is not the case for cross-sectional TEM images, presumably because the original structure is fixed and stabilized by the embedding resin against electron bombardment in this case. The observed decrease of the interlayer distance might be due to a partial rearrangement of the template molecules between the layers under the influence of the electron beam. This phenomenon, which cannot be induced thermally to that extent, can be sufficiently explained with the flexible paraffin-like arrangement of template molecules between the layers described above. Consequently, this effect is smallest for templates with short chains where there is practically no possibility for a paraffin-like packing because the observed interlayer spacings are too large (see above).

Selected images of rather well-developed VO$_x$−NTs obtained with different templates are represented in Figure 6. By far most of the tubes are open (Figure 6a,b). Occasionally, closed tubes can be found in all samples, almost independent of the template

**Table 3.** Exchange Reactions of Intercalated Monoamines by Diamines[a]

| | as−synthesized monoamine VO$_x$−NT | | diamine exchanged VO$_x$−NT | | |
|---|---|---|---|---|---|
| | | layer distance [nm] | | | |
| monoamine template | layer distance [nm] (XRD data) | diamine | XRD | ED |
| hexylamine | 2.00 | 1,12-diaminododecane | 1.84 | 1.5−1.6 |
| undecylamine | 2.62 | 1,12-diaminododecane | 1.83 | 1.8−2.0 |
| hexadecylamine | 3.35 | 1,12-diaminododecane | 1.86 | 1.6 |
| butylamine | 1.66 | ethylendiamine | 1.58 | |
| hexylamine | 2.00 | ethylendiamine | 1.3 | 1.0−1.1 |
| undecylamine | 2.62 | ethylendiamine | 1.6−1.7 | 1.3−1.4 |
| hexadecylamine | 3.35 | ethylendiamine | 1.5 | |
| octylamine | 2.24 | 1,20-eicosandiamine | 3.5 | |
| hexadecylamine | 3.35 | 1,6-diaminohexane | 1.52 | |

[a] Layer distances (determined from the *d* value of the 001 reflection, XRD data) of monoamine−VO$_x$−NTs before and after exchange with α,ω-diamines are also given.
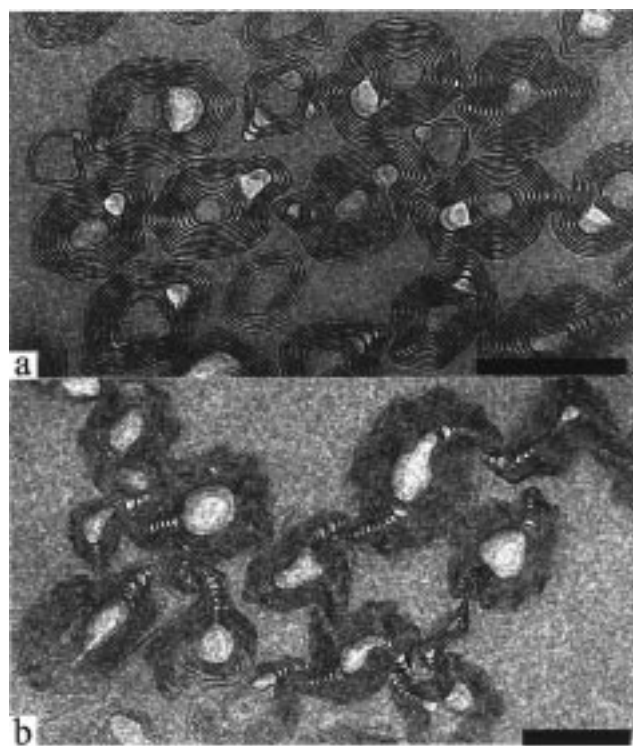


**Figure 7.** Cross-sectional TEM images of C$_{16}$−VO$_x$−NTs (a) and C$_{22}$−VO$_x$−NTs (b) serpentine-like scrolls are predominant. The inner cores of most C$_{22}$−VO$_x$−NTs (b) are empty. The length of the bars is 100 nm.

concentration or other synthesis parameters. They are terminated either by a section of parallel layers (about five in this case) oriented perpendicular to the walls such as a lid on a tin can (Figure 6c) or by a pointed cap of conically deformed layers (Figure 6d).

In general, the tube openings vary between 5 and 50 nm while the outer diameters range from 15 to 100 nm. However, there is a characteristic influence by the type of the amine: monoamine templates tend to form wide tube openings and tube walls consisting of rather few layers (2−10), whereas with diamines, tubes with a comparatively small inner diameter and with a much larger number of layers (>10) are predominant. This systematic influence of the templates on the tube morphology as revealed in longitudinal observation (cf. Figure 6) is also evident from the cross-sectional TEM investigation that directly shows the layer structure within the tube walls (Figures 3 and 7−9).

As is already apparent from the nonsymmetric fringe patterns of the walls observed in the longitudinal direction (Figure 2a),

cross-sections also exemplify that most nanotubes are not rotationally symmetric; depressions in the tube walls and holes therein appear frequently. It should be mentioned that these defects probably are not caused by the embedding and thinning procedure: in longitudinal TEM investigations, short tube fragments with the tube axis occasionally oriented parallel to the incident electron beam show similar distortions (Figure 8f).

The major fraction of the tubes has a serpentine-like morphology: they are single- or double-layer scrolls in most cases (Figure 8a,b). Tubes built up of concentric, closed cylinders ("ideal tubes") are rarely present (<1%). They are only observed if the tube wall comprises four or fewer layers (Figures 3a and 8c). The contrast is often blurred in some regions of the nanotube walls, which prevents a clear discernment between closed circles and scrolls. Sometimes, the layers are not closed to form concentric rings or helices, but appear as open circles (Figure 8d).

In the cross-sections, the inner core of VO$_x$−NTs with monoamine templates with alkyl chains less than 20 CH$_2$ groups long shows the same image contrast as the surrounding amorphous resin and is therefore completely filled, presumably with amorphous organic material (cf. Figure 8a). The presence of carbon in the tube core is also evident in the carbon map (Figure 3c). This filling prevents access to the inner surface of the tubes. A brighter contrast, which corresponds to that of a hole in the sample, is observed in distortions of tube walls, and thus, this site is indeed empty. Interestingly, the inner cores of a large proportion of C$_{20}$−VO$_x$−NTs and C$_{22}$−VO$_x$−NTs are apparently empty or only partially filled (Figures 7b and 8e).

Most diamine VO$_x$−NTs are multilayer scrolls with narrow cores and thick walls, composed of sheet packs of several vanadium oxide layers (predominantly five) (Figure 9). Occasionally, these packs can be closed to form concentric tubes.

The scroll-like structure of the tubes is the obvious reason for high structural flexibility, which is indicated by the readiness of exchange reactions (Table 3). For example, the enormous reduction of the sheet distance from 3 to 0.86 nm caused by exchange of the hexadecylammonium template with ammonium cations under preservation of the tube morphology[9b] can easily be rationalized with such a scroll structure but not with concentric tubes. The amine can be substituted by various metal cations,[23] e.g., Na$^+$, K$^+$, Mg$^{2+}$, Ca$^{2+}$, and Sr$^{2+}$, or via proton exchange with neutral diamines. These results are supported by the XPS studies mentioned above, which clearly show that the amine is protonated.

Intercalation of diamines by exchange against monoamines yielded tubes with a well-ordered layer structure and uniform distances throughout the tube length (Table 3). The inner diameters of these tubes have increased on the average by about
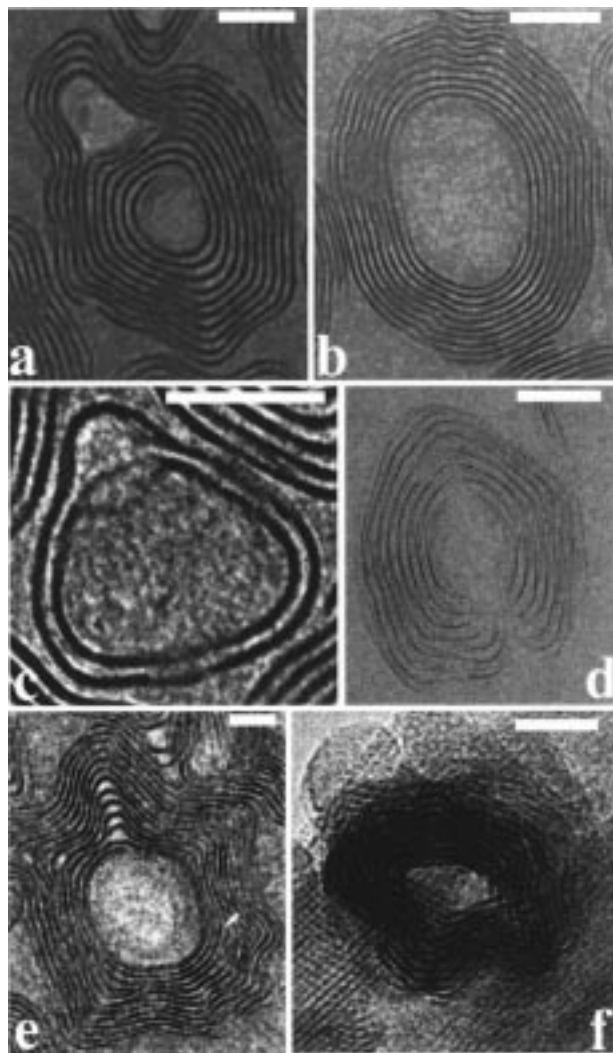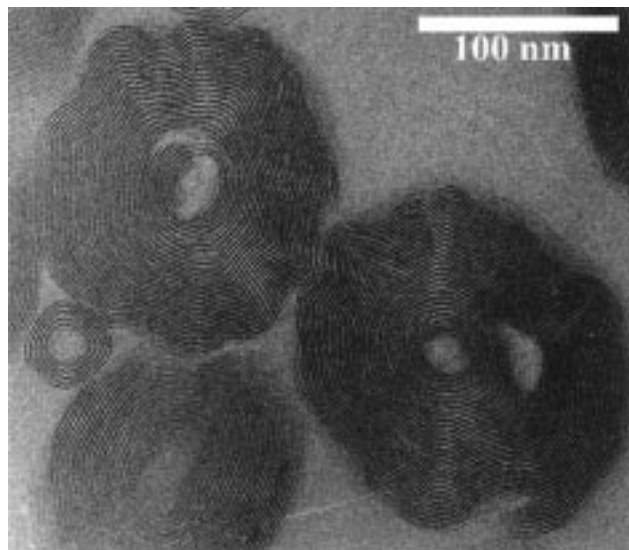
**Figure 9.** Cross-sectional TEM images of C$_{20}$−A−VO$_x$−NTs. The larger thickness of the tube walls as well as the smaller inner core compared to monoamine−VO$_x$−NTs is striking.

**Figure 8.** Different types of VO$_x$−NTs: (a) C$_{16}$−VO$_x$−NT: single-layer scroll. (b) Double-layer scroll of C$_{20}$−DA−VO$_x$−NT, obtained from C$_{16}$−VO$_x$−NT by a template exchange reaction with dodecyl-diamine. (c) C$_{16}$−VO$_x$−NT: concentric tube. (d) Incompletely closed C$_{12}$−VO$_x$−NT. (e) C$_{22}$−VO$_x$−NT: disordered scroll with an empty core. (f) This short fragment of a C$_{22}$−VO$_x$−NT nanotube was by chance oriented so that an observation along the tube axis was possible without applying the cross-sectional preparation. The disorder and distortions of the tube walls appears to be similar to that observed in the other images. Interestingly, the tube core seems to be empty. In all images, the length of the bar is 20 nm.

20%. In cross-sections, these tubes appear either as scrolls (Figure 8b) or, frequently, as open half cycles with a well-ordered sheet arrangement and without those holes which are often observed in VO$_x$−NTs with monoamines as templates. Apparently, an entropically driven exchange reaction of two monoamine molecules with one diamine molecule took place. This fact has been verified by elemental analysis of the exchanged products and thus further supports the structural model of paraffin-like stacking of template molecules between the vanadium oxide sheets.

## Conclusions

The preparation of new vanadium oxide nanotubes has been achieved via a two-step reaction: first, a gel is formed by the hydrolysis[24] and, second, the tubes are generated by hydrother-mal treatment. This reaction can be performed with a wide range

of primary amines and diamines, it is reproducible, and it leads with high selectivity to the tubes in excellent yield. The distance between the layers can be controlled by the length of the CH$_2$ chain of the amine template. The synthesis with diamine templates led to tubes with thicker walls and smaller inner cores compared with monoamine VO$_x$−NTs.

Although we could not yet propose a reliable model for the structure of the VO$_x$ layers, the presented experimental results point to a structure consisting of VO$_4$ tetrahedra and VO$_5$ square pyramids simultaneously. The square lattice with $a \approx 0.61$ nm possibly suggests a relationship to the tetragonal structures of α-V$_{1.08}$P$_{0.92}$O$_5$ ($a = 0.601$ nm),[25] (NH$_4$)$_2$V$_3$O$_8$ ($a/\sqrt{2} = 0.629$ nm),[26] K$_2$V$_3$O$_8$ ($a/\sqrt{2} = 0.627$ nm),[27] or BaV$_7$O$_{16}$·$n$H$_2$O ($a = 0.616$ nm).[28]

Compared with the steadily growing family of mesoporous metal oxides with a lamellar structure, the VO$_x$−NTs are different not only because of their tubular morphology but also because of their well-structured walls. A pure tubular vanadium oxide is not accessible by removing the template molecules from the tubes since a thermal treatment at temperatures higher than 250 °C destroys them completely. A more promising approach especially with respect to possible applications represents the functionalization of the tube walls by substitution of the protonated organic template by alkali or alkaline-earth metal cations. The flexibility of the structure provides an outstanding potential for a far-reaching tailoring of the nanotube structure connected with a modification of the mechanical, electrical, and chemical properties.

(24) Livage, J. *Chem. Mater.* **1991**, *3*, 578.

(25) Jordan, B. D.; Calvo, C. *Acta Crystallogr. B* **1976**, *32*, 2899.
(26) Theobald, F. R.; Theobald, J. G.; Vedrine, J. C.; Clad, R.; Benard, J. *J. Phys. Chem. Solids* **1984**, *45*, 581.
(27) Galy, J.; Carpy, A. *Acta Crystallogr. B* **1975**, *31*, 1794.
(28) Wang, X.; Liu, T.; Bontchev, R.; Jacobson, A. J. *J. Chem. Soc., Chem. Commun.* **1998**, 1009.